Quenching and Blinking of Fluorescence of a Single Dye Molecule Bound to Gold Nanoparticles

Fabio Cannone and Giuseppe Chirico*

Laboratory for Advanced BioSpectroscopy (LABS), INFM-CNR, Physics Department, University of Milano-Bicocca, Milano I-20126, Italy

Anna Rita Bizzarri* and Salvatore Cannistraro

Biophysics and Nanoscience Centre, INFM-CNISM, Dipartimento di Scienze Ambientali, Università della Tuscia, I-01100 Viterbo, Italy

Received: April 27, 2006; In Final Form: June 21, 2006

A fluorescein derivative (SAMSA) bound to gold nanoparticles of different diameters is investigated by time-resolved fluorescence at the single molecule level in a wide dynamic range, from nanosecond to second time scale. The significant decrease of both SAMSA excited state lifetime and fluorescence quantum yield observed upon binding to gold nanoparticles can be essentially traced back to an increase of the nonradiative deactivation rate, probably due to energy transfer, that depends on the nanoparticle size. A slow single molecule fluorescence blinking, in the ms time scale, has a marked dependence on the excitation intensity both under single and under two photon excitation. The blinking dynamics is limited by a low probability nonlinear excitation to a high energy state from which a transition to a dark state occurs. The results point out a strong coupling between the vibro-electronic configuration of the dye and the plasmonic features of the metal nanoparticles that provide dye radiationless deactivation channels on a wide dynamic range.

Introduction

Systems consisting of dye molecules and noble nanoparticles (NPs) have recently gained considerable interest in photonics, optoelectronics, and material sciences[1] for their potential technological impact (solar cells, light harvesting, emitting devices, and so on).[2−4] Noble metal NPs are among the most polarizable inorganic templates capable of producing an enhanced optical field near their surfaces under visible electromagnetic radiation. When located in close proximity of a metallic NP, a dye exhibits strong changes in its electronic and optical properties, likely as a result of a mixing of the molecule and metal electronic levels as well as an interaction of the molecule with the surface plasmon resonance, which are modulated by the metal NP size.[3] Most notably, adsorption of a dye on a metal surface results in a quenching of its fluorescence, while a fluorescence enhancement has been reported when the dye is located at distances higher than 10 nm from the metal surface,[5−7] as was also recently demonstrated experimentally.[8] Furthermore, molecules placed on rough metal surfaces exhibit a drastic increase in the Raman cross section (surface-enhanced Raman scattering)[9−12] and in the electronic transition excitation rate.[8] Besides the implications for molecular electronic applications of hybrid NP−dye devices, studies of the fluorescence quenching could, therefore, provide a deeper understanding of other underlying photophysical phenomena, leading to higher spectroscopic sensitivity.

The fluorescence dynamics of dyes in proximity to metal NPs has been recently investigated in bulk solutions.[6] However, bulk measurements provide ensemble-averaged quantities and could, therefore, mask specific phenomena occurring at the molecule−metal interface so that a detailed picture of the dynamics of the system might not be obtained.[13,14] Single-molecule spectroscopy (SMS) has therefore emerged as a powerful method to probe the electronic excited states, spectroscopic fluctuations, and molecular dynamics of single molecules (SM) near metal surfaces.[15,16] Very recently, studies of the fluorescence emission rate of single dyes versus the metal nanoparticle−dye distance have been reported and compared successfully to a theoretical treatment based on multipole approximations of the light-induced electric fields.[8]

Two main approaches to the study of the fluorescence dynamics of single dye molecules bound to metal NPs have been reported. The shortening of the excited-state lifetime, down to a few hundreds of picoseconds, has been measured and ascribed either to energy[6] or to electron-transfer[17] processes. Alternatively, the blinking of fluorescence that occurs on a variety of time scales, from seconds to hundreds of microseconds, has been interpreted in terms of electron transfer from the dye to the noble metal nanoparticle.[4,18] Therefore, both fluorescence quenching and blinking, with widely different time dynamics (from hundreds of picoseconds to seconds), have been ascribed to electron transfer. However, rare direct experimental evidence of the charge-transfer role in the observed phenomena have been brought.[19] The simultaneous investigation of the fluorescence blinking and quenching or excited-state lifetime shortening is the aim of the present report.

Time-resolved fluorescence, pushed down to the level of SM has been applied here to study, in a wide time window (from ns to s), the fluorescence dynamics of SAMSA, an organic dye derived from fluorescein. SAMSA bears an activable thiol group (−SH), which can be exploited for binding gold NP under

* To whom correspondence should be addressed. E-mail: bizzarri@unitus.it (A.R.B.); giuseppe.chirico@mib.infn.it (G.C.).

10.1021/jp0625816 CCC: $33.50
Published on Web 08/02/2006

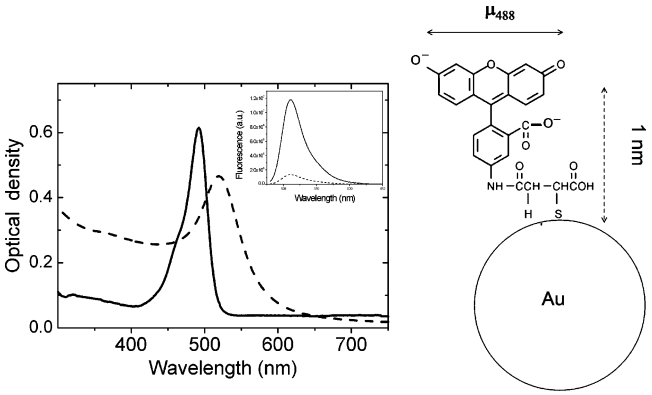

Figure 1. Optical density spectra of SAMSA (continuous black line) after activation of the thiol group, of gold NPs (dashed black line), and of gold NPs incubated with SAMSA (continuous gray line). [SAMSA] ≅ 8 μM. Inset: fluorescence emission spectra of bulk SAMSA (**c**ontinuous line) and of SAMSA bound to gold colloids 20 nm in diameter (dashed line), excited at 470 nm. Chemical structure of activated SAMSA (in the dianionic form expected in basic conditions, pH > 7) bound to gold NP. The diameter of the nanoparticle is not in scale with the molecule. The direction of the transition dipole for the 488 nm absorption band is indicated by a double arrow.

controlled topological and conductive conditions.[20] The measured fluorescence lifetimes, the quantum yields, and the temporal behavior of the on−off blinking of single SAMSA molecules conjugated to gold NPs of different sizes, have been measured and correlated to the photophysical processes occurring at the metal interface. Our purpose here is to measure both excited state lifetimes and blinking times on SM attached to gold NPs and to correlate them to the fluorescence quantum yield. By proving the photoactivation of the observed fluorescence blinking and by trying to elucidate the role of the excitation rate in the observed slow blinking dynamics, we envision possible sources for the widely different fluorescence dynamics reported in the literature for dye−metal NP systems.

Materials and Methods

Materials. SAMSA (Molecular probes, A-685) in the amount of 10 mg was dissolved in 1 mL of 0.1 M sodium hydroxide and incubated for 15 min to remove the acetyl group protecting the thiol. The solution was then neutralized with 6 M chloridric acid and buffered with sodium phosphate at pH = 7. Gold colloids were purchased from Sigma (Sigma, St. Louis, MO 63103): diameter 5 nm, G 1402; diameter 10 nm, G 1527; diameter 20 nm, G 1652). Clean glass 7 × 1.5 × 0.04 cm was silanized by reaction with 0.15% v/v triethoxymethysilane (CH_3-$Si(OC_2H_5)_3$, 69435 Sigma) in chloroform (Aldrich, 13,295-0). The reaction was allowed to proceed for 15 min at room temperature (21 °C).[21] SAMSA should attach to gold mainly via thiol bonding.[22] As a result of the substantial repulsion of the COO^- and O^- groups from gold,[23] it is likely that the planar moiety of SAMSA (dianionic at pH > 7) lies perpendicular to the gold NP surface, as indicated in Figure 1.

Methods. *Absorption Spectra.* Optical absorption was measured by using a Jasco V-550 UV/visible spectrophotometer. Bulk steady-state fluorescence emission spectra were measured at room temperature (Spex FluoroMax, Jobin Yvon, France).

Two-Photon Excitation Microscopy. For fluorescence microscopy, two-photon excitation was employed[24] with excitation at 790 nm (80 MHz repetition rate, 220 fs pulse width, and 0.5 mW estimated power on the sample). The experimental setup is built around an inverted microscope (TE300, Nikon, Firenze, Italy) and a nanocube x−y−z piezo-actuator (Physik Instrumente, Milano, Italy).[25] A portion of the laser beam is collimated to the epi-fluorescence port of the microscope and is rejected by a dichroic mirror (650 DCSPRX C72-38; Chroma, Inc., Brattelboro, VT) into the objective (N.A. = 1.3, Plan Apochromat 100× oil, Nikon).

Single-Photon Excitation Microscopy. The optical setup for the single-photon imaging experiments is based on an inverted microscope (Olympus IX2 Confocal Microscope, Olympus), a FluoView 1000 scanning head and an air-cooled argon laser exciting at 488 nm. The laser beam is sent to the entrance pupil of the objective (N.A. = 1.4, Plan Apochromat 100× oil, Olympus, Japan) by the scanning lens. The fluorescence signal, collected by the same objective, is selected by a band-pass filter (HQ520-50, Chroma, Inc., Brattelboro, VT).

Two-Photon Fluorescence Images. The acquisition of the images (30 × 30 pixels) with 1-ms residence time per pixel takes ≅ 1 s. The field of view employed is 6 × 6 μm^2, and the excitation power is usually ≅ 10 kW cm^{-2} on the sample (λ_{exc} = 790 nm). The fluorescence emission is selected by a band-pass filter at λ_{em} = 520 nm (HQ520-50, Chroma, Inc., Brattelboro, VT). The pixel linear size (200 nm) is close to the point spread function (PSF) width of our experimental setup (280 ± 60 nm).[22] The image acquisition is performed by means of a home-coded software developed in Labwindows/CVI (National Instruments, Milano, Italy).[22]

Single-Photon Confocal Images. The radial and the axial resolutions of the confocal setup are 250 ± 10 nm and 1000 ± 80 nm, as measured on 64 nm spheres in glycerol (n = 1.417) with a 50 μm pinhole at 488 nm. The acquisition of the images (512 × 512 pixels, dwell time = 2.0 μs per pixel) takes ≅524 ms, with an estimated light intensity on the sample ≅20 μW. Fluorescence and transmission (differential interference contrast) images are acquired on the same field of view by the FluoView 1000 scanning head system.

Time-Resolved Fluorescence on SM. The two-photon fluorescence dynamics of SM was followed at millisecond time resolution by pointing the excitation beam directly on the spot coordinate obtained from a first fast image of the field of view. The stability of the microscope stage in the z-direction has been assessed by taking 140 × 140 μm^2 images right before and after the kinetics on a 10−15 μm field of view and by verifying that only the spot on which the kinetics was performed was missing in the second 140 × 140 μm^2 image. The stability of the signal was found to be ≅0.4% on a 100 s kinetics.

Excited-State Lifetime Measurements. The excited state lifetime was measured by means of a PCI board for time-correlated single-photon counting (Time Harp 200, PicoQuant, D) connected to an Avalanche photodiode (Perkin-Elmer, Canada, model SPCM-AQR15) directly coupled to the bottom port of the microscope in the two-photon excitation set up. Each acquisition run (duration = 4 s) corresponded typically to 50 000−120 000 photons at room temperature. The total number of background photons collected in the duration time is ≅2000. The impulse response function (IRF) was measured by exciting at λ_{exc} = 990 nm urea dried on a glass slide and collecting the second harmonic generated signal at λ ≅ 495 nm (emission filter at 495 ± 10 nm) very close to the SAMSA emission wavelength (515 nm). The half-height full width of the IRF is ≅ 700 ps (Figure 2). All the fluorescence decays have been deconvolved with the IRF by means of the FLUOFIT code (Picoquant, Berlin, D).

Results and Discussion

Absorption and Fluorescence Emission of Bulk Solutions. Figure 1 shows the optical spectrum of: (i) an 8 μM SAMSA

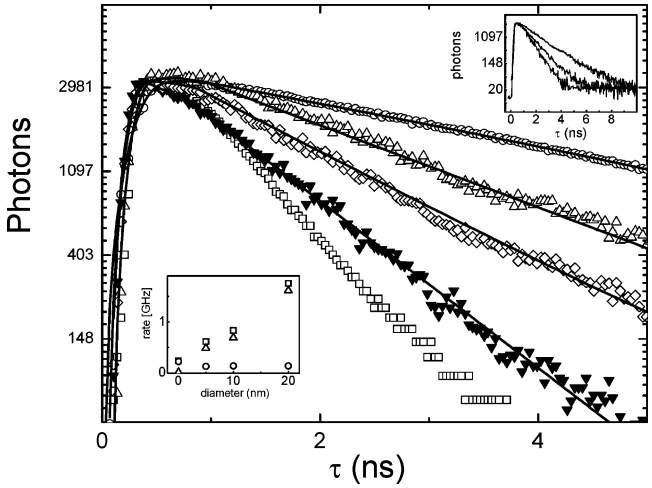

Figure 2. Time-resolved fluorescence emission of SM of free SAMSA (open circles) and of SAMSA bound to gold colloids (open triangles, 5 nm; diamonds, 10 nm; filled triangles, 20 nm) and the instrument response function, IRF (open squares). The solid lines are the best fit of the data obtained by convoluting a single exponential with the IRF, as described in the text. Upper inset: Time-resolved fluorescence emission of SM of SAMSA bound to 20 nm and to 10 nm gold colloids and the IRF (from top to bottom) over an extended acquisition time window. Lower inset: fluorescence rates: excited-state de-excitation rate, k (squares), radiative rate, k_{rad} (circles), and nonradiative rate, k_{nr} (triangles).

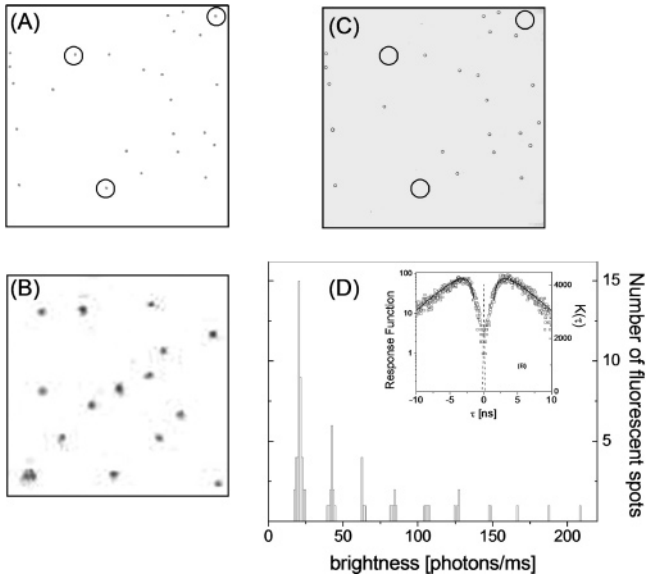

Figure 3. (A) Single-photon excitation fluorescence image (confocal setup) showing a typical field of view (20 × 20 μm) of SAMSA−colloid (5 nm in diameter) on silanized glass (λ_{exc} = 488 nm, excitation intensity ≅ 50 kW/cm^2). (B) Two-photon excitation fluorescence image showing a typical field of view (10 × 10 μm) of SAMSA−colloid (5 nm in diameter) on silanized glass under excitation at λ_{exc} = 790 nm, excitation intensity ≅ 100 kW/cm^2. Not all the spots correspond to single molecule emission. The spots that correspond to ≅22 photons/ms (see histogram in panel D) display a single-step fluorescence bleaching. (C) Transmitted light image of the same field of view represented in panel A. The spots observed in the image have the size of the PSF and correspond to the gold NPs. (D) Distribution of the fluorescence signal of the spots observed on images (panel B). Inset: probability density, $K(\tau)$, to detect two consecutive fluorescence photons at time lag τ (open squares) in the emission of single SAMSA on 5 nm gold colloids, showing antibunching at lag time ≅ 0 ns. The solid lines are the best fit to a double exponential function $-8260\exp[-\tau/\tau_1] + 10\,500\exp[-\tau/\tau_2] - 0.22$, with times $\tau_1 \cong 4.2$ ns and $\tau_2 \cong 18$ ns. The dashed line (left axis) represents the response function of the system obtained by electronically spitting the signal of a single detector.

solution (continuous black line), (ii) a 20 nm gold NP solution (1:1 stoichiometry, dashed black line), and (iii) a 20 nm NP solution after incubation with SAMSA molecules (continuous gray line). The colloids volume fraction is ≅0.02, and therefore, the particle light scattering from colloids negligibly affects the absorption and emission spectra. Practically no changes are observed in the NP optical spectrum after incubation with SAMSA molecules; such a spectrum being dominated by the surface plasmon resonance peaked at about 520 nm[3]. The inset of Figure 1 shows the fluorescence emission, upon excitation at 470 nm, of a 0.1 μM solution of free SAMSA (continuous line) and of SAMSA bound to 20-nm gold NPs (dashed line). A drastic lowering of SAMSA fluorescence is detected upon binding to gold NPs (a similar behavior is observed for NPs of 5 and 10 nm, not shown).

The presence of a thiol group in the proximity of a gold surface ensures a binding between the dye and the gold nanoparticle.[26] Other groups, such as amines or unsaturated carbon bonds, might also interact with gold. In our case, the dominant role of the thiol group in the gold−dye interaction has been checked by performing a control experiment with a thiol-free fluorescein. In such a case, the fluorescence emission is dominated by free fluorescein, indicating that thiol−gold interaction is dominating the dye−nanoparticle binding. Regarding the orientation of the excitation dipole (488 nm excitation wavelength) with respect to the gold NP surface, we observe that the repulsion between the charged carboxylic and oxidrilic moieties and the gold ensures a preferential orientation of the dye, as reported in the scheme of Figure 1.[23] Moreover, the excitation dipole moment of SAMSA for the 488 nm absorption band is presumably parallel to the xanthene ring as in fluorescein[27] and, therefore, is parallel to the gold surface.

Single-Molecule Imaging of SAMSA. We have studied fluorescence emission of single SAMSA molecules bound to gold NPs (at stoichiometry = 1:1) on silanized glasses. The pH of the samples was controlled by keeping them hydrated with phosphate buffer at pH = 8.2. A typical emission image of such a sample (5 nm gold colloids) under one- (Figure 3A) and two-photon excitation (Figure 3B) shows well-defined spots of the size of the microscope PSF.[25] The spots visible in the transmitted light images (Figure 3C; λ_{exc} = 488 nm) are ascribed to 5 nm gold colloids. A comparison between Figure 3C and Figure 3A shows that some fluorescent spots have no corresponding signal in the transmitted light image (circles in Figures 3A and 3C). Such spots are ascribed to free SAMSA, that is, dye not bound to a gold NP. This assumption is confirmed by the analysis of the fluorescence molecular brightness. SM emission has been checked in three different ways. First, the levels of the fluorescence emission rate of the spots were analyzed, finding well distinct peaks that correspond to multiples of a common value of fluorescence rate (Figure 3D). Such a value was assumed to be the molecular brightness (photons/second/molecule) of single SAMSA molecules bound to gold NPs. Second, only those spots that displayed a single-step drop of the fluorescence signal to the background level were assumed to be SM (see hereafter, Figure 4, top trace of panel A, as an example). Third, when performing antibunching experiments, we found that the probability density, $K(\tau)$, to detect two consecutive fluorescence photons at time lag τ (inset of Figure 3D) has an anticorrelation dip at $\tau \cong 0$ ns. All these findings provide evidence that only one fluorophore molecule is emitting.[28,29]

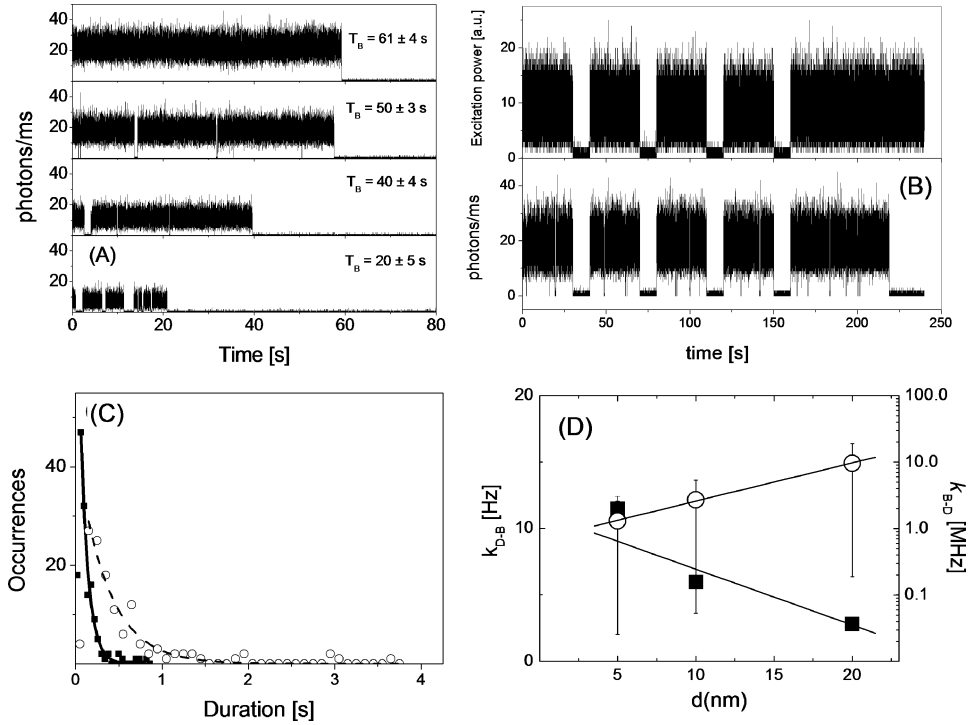

Figure 4. (A) Traces of fluorescence versus time of SM of free SAMSA and of SAMSA bound to gold colloids of increasing diameter: 0 (free SAMSA), 5, 10, and 20 nm, from top to bottom. Excitation intensity ≅ 100 kW/cm^2. The average bleaching time, T_B, is reported in the panels. (B) Interleaved excitation experiments on single SAMSA bound to a 5 nm gold colloid. Upper panel shows the output of a photodiode measuring a small portion of the exciting laser beam. Lower panel shows the fluorescence counts measured from a single SAMSA. (C) Intensity histograms of the on- and off-times computed on 30 single SAMSA molecules bound to 5 nm (filled squares) and 20 nm (open circles) gold colloids. The solid lines are single-exponential fit to the data. The average on- and off-times for the whole series of colloid sizes are reported in the plot. (D) Blinking rates: $k_{B\rightarrow D}$ (open circles) and $k_{D\rightarrow B}$ (solid squares). Bars on $k_{B\rightarrow D}$ correspond to the range $\sigma_{(4)} \cong 10^{-112} - 10^{-110}$ (cm^2 s)^4/s/photons^3 for the four-photon cross-section process presumably involved in blinking. Standard errors for $k_{D\rightarrow B}$ are smaller than the symbol size.

Single Molecule Excited-State Lifetime. Fluorescence dynamics of single SAMSA molecules, both free and bound to gold NPs, was first studied at nanosecond time resolution. Figure 2 shows the time-resolved fluorescence emission of single SAMSA molecules bound to gold NPs of increasing size. Data best fitting yields a monoexponential decay for both free and NP-bound single SAMSA molecules (≅50 SM investigated). The excited-state lifetime of free SAMSA at the emission wavelength $\lambda_{em} = 520$ nm, is $\tau = 4.1 \pm 0.1$ ns, as found in solution.[30] A significant shortening of τ is observed upon binding of SAMSA to gold.[31] Moreover, τ progressively decreases with the increase of the NP dimension: $\tau = 1.62 \pm 0.07$, 1.20 ± 0.07, and 0.57 ± 0.06 ns for NP diameters of 5, 10, and 20 nm, respectively. The excited-state lifetimes display a Gaussian distribution with a width that is very close to the Poisson statistical uncertainty determined by the limited number of photons collected per decay. Therefore, no clear heterogeneity is evident from the collected data. It must be noted also that the background noise contribution is at most ≅ 3% in the case of the most-quenching colloids (20 nm in diameter) and that its contribution can be clearly discerned from the comparison of the fluorescence decay of the most-quenched dyes (20 nm gold NP) with the IRF, as shown in the inset of Figure 2. These results are confirmed by bulk measurements on ≅30 μM SAMSA concentration and the ratio of [gold NPs]/[SAMSA] = 30.

The fluorescence rate *k(d)*, which is dependent on the particle diameter *d* and defined as the inverse of the measured decay time, can be expressed in terms of the radiative $k_{rad}(d)$ and nonradiative $k_{nr}(d)$ rates

$$\tau(d)^{-1} = k(d) = [k_{rad}(d) + k_{nr}(d)] \qquad (1)$$

which are, in turn, related to the fluorescence quantum yield by

$$\phi = k_{rad}(d)/k(d) \qquad (2)$$

Hence, a measure of ϕ from the single-photon emission curves would provide the values of k_{rad} and k_{nr}.

Quantum Yield Measurements. Quantum yield measurements were performed on SAMSA bound to gold NP and spread over glass substrates by spin coating: the area of the fluorescence emission spectrum of dye samples at constant absorbance was compared to that of a reference dye of known quantum yield.

Now the problem is to select only the fluorescence signal coming from SAMSA bound to metal NPs, getting rid of the contribution from uncomplexed SAMSA. The fluorescence signal from SAMSA−gold colloid samples at a stoichiometric ratio < 20:1 is in fact affected by the contribution of uncomplexed SAMSA, as shown in Figure 5, where the fluorescence emission and absorption of 30 μM SAMSA solutions spread in thin films on glass slides, is shown to decrease markedly with the stoichiometry ratio R_p = [gold NPs]/[SAMSA] and, therefore, with the percentage of complexed dyes in solution. This fact implies an underestimation of the quenching of the SAMSA fluorescence upon binding to gold NPs.

According to the data trend reported in Figure 5, we assume that at stoichiometry [gold NPs]/[SAMSA] = 30:1 most of the SAMSA dyes are complexed to gold NPs. The fluorescence quantum yield was then measured from the area of the emission spectrum ($\lambda_{exc} = 488$ nm) of SAMSA bound to gold NPs at $R_p = 30$ on silanized glasses, compared to that measured for fluorescein at pH = 10[30] at constant sample absorbance. By assuming $\phi = 0.96$ for free fluorescein, we estimated $\phi = 0.92$

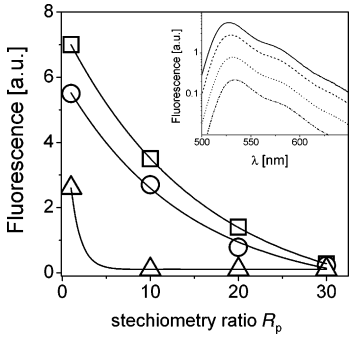

Figure 5. Fluorescence emission of thin films obtained from SAMSA−NP solutions at an increasing stoichiometry ratio R_p = [gold NP]/[SAMSA] = R_p and [SAMSA] = 30 μM. SAMSA emission at λ_{em} = 525 nm under excitation at λ_{exc} = 488 nm versus R_p for complexes with gold colloids of 5 nm (squares), 10 nm (circles), and 20 nm (triangles) in diameter. Solid lines are an exponential fit, shown to guide the eye. Inset: fluorescence emission spectra (single-photon excitation at λ_{exc} = 488 nm) of SAMSA complexed to 10 nm gold NP at R_p = 1 (solid line), 10 (dashed line), 20 (dotted line), and 30 (dot−dashed line).

± 0.09, 0.21 ± 0.03, 0.17 ± 0.02, and 0.08 ± 0.02 for free SAMSA and for SAMSA bound to NPs of diameters 5, 10, and 20 nm, respectively.

Two-Photon Cross-Sections. The values of the two-photon cross-sections, $\sigma_{(2)}$, for SAMSA free and bound to the gold NPs were estimated from the slope of the dependence of the two-photon excited fluorescence rate on the excitation intensity ($\cong \alpha I_{EXC}^2$) compared to that measured for rhodamine 6G in ethanol, taken as a reference. The fluorescence quantum yield ϕ was evaluated as described above and assumed to be unaffected by the nonlinear excitation process.[32] The estimate of the two-photon cross-section relative to a reference dye can then be gained from the ratio $\alpha_{dye}\phi_{ref}/\alpha_{ref}\phi_{dye}$. In these measurements, the excitation intensity was kept ≅100 kW/cm^2, and the pulse width measured on the sample plane[33] was ≅230 ± 30 fs. By assuming $\sigma_{(2)} \cong$ 135 GM (GM = Göppert−Mayer = 10^{-50} cm^4 s/photons) for rhodamine 6G in ethanol,[34] we estimated $\sigma_{(2)} \cong$ 35 ± 3 GM for free SAMSA and $\sigma_{(2)} \cong$ 110 ± 10 GM for SAMSA bound to gold NPs. The value of the two-photon cross-section of the bound dye is then about three times that measured for free SAMSA and was found to be independent of the NP diameter. This is in agreement with two-photon absorption enhancement in dyes close to metal surfaces recently reported.[35] Therefore, the observed reduction in the overall fluorescence output is actually related to a reduction in the quantum yield, which is partially compensated by the increase in the two-photon cross-section. This finding could be of general interest for a dye−metal NP system, as also evidenced in ref 8.

Radiative and Nonradiative Rate Constants. From the experimental values of ϕ and τ and eqs 1 and 2, we can then compute k_{rad} and k_{nr} as functions of the NP diameter, d, as shown in the inset of Figure 2 and in Table 1. Binding of SAMSA to gold NPs yields a strong increase in k_{nr} with respect to free SAMSA; such an effect being progressively higher with increasing the NP diameter. Conversely, k_{rad} of SAMSA bound to gold NPs is slightly lower than that of free SAMSA and remains almost constant with d. The $k_{nr}(d)$ trend suggests that additional relaxation channels become available to the excited fluorophore upon binding to the metal NP, resulting in faster radiationless deactivation pathways observed at the SM level.[36] Furthermore, while the trend of k_{rad} with the NP size finds a good correspondence with the Gersten−Nitzan (GN) model,[37] the $k_{nr}(d)$ appears drastically lower than the estimated values from this model (Table 1). Such a discrepancy, which finds a correspondence with that found in ref 6, suggests that the static GN model based on a description of the molecules at the metal surface in terms of Hertzian dipole emitters that suffer energy transfer, does not provide a complete description of the observed phenomenon. Because the dye−metal interaction depends on the relative orientation of the molecular excitation dipole and the nanoparticle surface, we have always assumed, for the theoretical predictions of the de-excitation rates, that the SAMSA excitation dipole is parallel to the gold NP surface (scheme in Figure 1).

TABLE 1: Radiative and Nonradiative De-Excitation Rates for SAMSA Bound to Gold NP[a]

d (nm)	$k \times 10^8$ [Hz]	$k_{rad} \times 10^8$ [Hz]	$k_{nr} \times 10^8$ [Hz]	$k_{rad}^{GN} \times 10^8$ [Hz]	$k_{ET}^{GN} \times 10^{12}$ [Hz]
0	2.4 (0.06)	2.2 (0.2)	0.2 (0.1)	2	0
5	6.2 (0.3)	1.3 (0.2)	4.88 (0.3)	0.08	3.1
10	8.3 (0.5)	1.4 (0.2)	6.9 (0.5)	0.447	3.25
20	17.5 (1.2)	1.4 (0.3)	16.1 (1.3)	0.944	3.3

[a] Total, radiative, and nonradiative de-excitation rates derived from the measurements of the quantum yield and the excited-state lifetime reported in the text. Diameter d indicates the gold NP diameter in nm. The k_{rad}^{GN} and k_{nr}^{GN} are the radiative and nonradiative (resonant energy transfer), computed from the Gersten−Nitzan (GN) model.[37] The numbers in parentheses are the standard deviation on the data.

Very recently, it has been shown that the dipole approximation model fails at dye−NP distances smaller than the light wavelength.[8] A multipole expansion of the fields indicates that in the present case only fluorescence quenching is expected due to the small size of the gold NPs. In our case, the dye is adsorbed on the gold NP surface at an estimated distance of ≅1 nm. We have assumed that a better theoretical description of the process should also take into account the high polarizability of the gold particle and the possible coherent coupling of the excited states of SAMSA and the bound electronic transition dipoles of gold.[38]

Single-Molecule Fluorescence Blinking. With the aim to closer address the nonradiative mechanisms for our system, we have then followed the photodynamics of SAMSA bound to the metal NPs in the ms−s time regime. To this purpose, we have exploited the capability of our setup to follow, even for relatively long times, low quantum yield excited-state deactivation processes.[25,39] Free SAMSA molecules displayed a single emission level before a sudden one-step drop of the signal to the background level (Figure 4A, upper panel). SAMSA molecules bound to gold NPs displayed a number of fluorescence flickering before a permanent (dark time larger than 60 s) loss of fluorescence occurred (Figure 4A, lower panels). The average duration of the emission (photobleaching time, T_B), is registered for free and bound SAMSA (Figure 4A), finding that T_B becomes significantly lower with increasing the diameter of the NP and strongly correlates with the corresponding fluorescence lifetime decrease. By performing second harmonic generation images of the gold colloids under excitation at λ_{exc} = 970 nm, we have verified that the colloids were found at the same position at which the SAMSA fluorescence signal was recorded, even after the SAMSA dye has undergone irreversible bleaching. The origin of bleaching is likely to be due to thermal effects,[40] as indicated by the lengthening of the duration of the fluorescence emission observed under alternate excitation, as reported in Figure 4B. In this experiment, the laser excitation is periodically shut, therefore, leaving the dye the time to relax possible thermal loading. The total duration of the fluorescence emission decreases rapidly with the excitation duty cycle.

TABLE 2: On- and Off-Average Blinking Times[a]

d (nm)	$\langle\tau_{on}\rangle$ [s]	$\langle\tau_{off}\rangle$ [ms]
0		
5	6.8 ± 0.6	90 ± 7
10	5.6 ± 0.4	170 ± 15
20	2.7 ± 0.2	360 ± 30

[a] Fluorescence blinking on- (τ_{on}) and off-times (τ_{off}) of SAMSA free ($d = 0$ nm) and bound to gold NPs of increasing diameter, d.

Regarding the fluorescence dynamics, SM traces from SAMSA molecules bound to gold NPs show a number of fluorescence flickering events. Such on−off blinking, *which are visible only on SAMSA molecules bound to gold NPs* (Figure 4A) *and never observed on free SAMSA on silanized glasses*, could be generally ascribed to several processes such as triplet state population, molecular diffusion processes, conformational transitions, and also reversible electron transfer.[41] The average blinking times of the on (τ_{on}) and off (τ_{off}) states have been measured from fluorescence traces according to the procedure reported in refs 36, 41, 42. The τ_{on} and τ_{off} distributions, computed on a set of 50 single SAMSA molecules under excitation intensity $I_{exc} \cong 100$ kW/cm^2, shown in Figure 4C. In all cases, the histograms can be successfully described by single-exponential curves, suggesting that the blinking is due to a single relaxation process. The on and off times (Table 2) are on the order of a few seconds and a few hundreds of ms, respectively. τ_{on} shows a systematic decrease from ≅6 to ≅2 s, at a variance with τ_{off} that increases from ≅ 90 to ≅ 350 ms, when passing from $d = 5$ to $d = 20$ nm. On the other hand, interleaved excitation experiments, such as those reported in Figure 4B, indicate no systematic dependence of τ_{on} and τ_{off} on the excitation duty cycle and, therefore, thermal load is unlikely to affect the blinking times.

The blinking on- and off-times have markedly different dependence on the excitation intensity: while the off-time does not vary appreciably with I_{exc}, the blinking on-rate, $k_{on} = 1/\tau_{on}$, under two-photon excitation increases as $I_{exc}^{4.2\pm0.2}$ (Figure 6). On the other hand, the molecular brightness follows a second power law versus I_{exc} (Figure 6). These observations suggest that the fluorescence emission is primed by a two-photon transition, while the blinking process is likely to be photoactivated by two consecutive two-photon absorptions to a high-energy excited state (S2 in Figure 6). The steep dependence of k_{on} on the excitation intensity, which is the major support to the scheme reported in Figure 6, has been confirmed by single-photon excitation experiments performed on a confocal setup under 488 nm laser excitation. In this case, k_{on} is found to scale as $I_{exc}^{2\pm0.2}$, while the emission rate scales linearly with the excitation intensity.

The interaction of the dye with the gold NPs can occur from both the S1 and S2 excited states (see scheme in Figure 6). As for the dye−gold interaction from the S1 excited state of the dye, the main mechanism could be a nonradiative energy transfer to electrons at energies close to the gold Fermi level in the conduction band. These processes would lead to an increase in the total nonradiative rate of the dye from S1, with a consequent reduction of the excited-state lifetime and the quantum yield, as observed here. Regarding the blinking process, which we ascribe in the scheme of Figure 6 to the S2−gold NP interaction, the relaxation to the ground state leading to the on-transition, and determining the τ_{off}, is likely to be due to dissipative relaxation processes of the gold NP plasmons[43] or to charge back transfer, depending on whether the blinking transition is due to a nonradiative transfer to the gold surface plasmons or

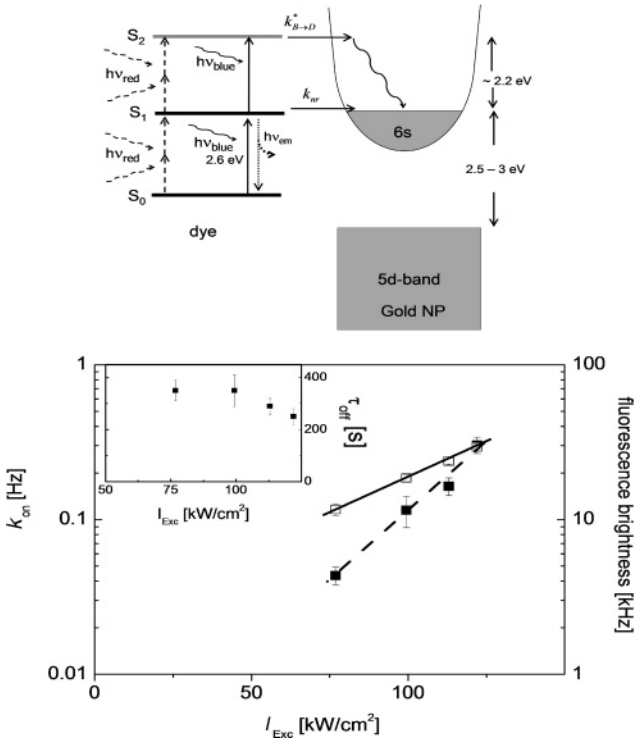

Figure 6. Upper panel: scheme of the dye−gold NP interactions. The dye one-photon and two-photon excitations are represented by continuous and dashed vertical arrows. The dye−gold NP interaction from S1 level is responsible for the nonradiative transfer to electrons in the conduction band of gold. The dye−gold NP interaction from S2 level is likely related to excitation of gold plasmons. Lower panel: dependence of the blinking on-rates, $k_{on} = 1/\tau_{on}$ (filled squares, left axis) and the fluorescence molecular brightness (open squares, right axis) versus the excitation intensity. The solid lines are a fourth (dashed line) and a second (solid line) power law fit to the data. Inset: off-times versus the excitation intensity.

to a charge transfer to the gold NP high energy levels in the gold 6s conduction band. Actually, the observation of a slow recovery rate from the dark state suggests that the dye−gold NP system is a highly coupled complex in which the recovery of the dye bright state from S2 is limited by the gold NP energy relaxation through a variety of channels. For this reason, we prefer not to specifically draw a back transition channel in Figure 6.

Finally, it is important to note that SAMSA uncomplexed to the gold NPs, does not show fluorescence blinking when laid on a silanized glass surface. Moreover, no detectable fluorescence emission from gold NPs alone has been detected upon two-photon excitation in the range 750−960 nm, while a dim emission at 560 nm under single-photon excitation at 543 nm and a nonlinear excitation at 960−980 nm (second harmonic generation) have been detected.

Because the dark to bright (D → B) blinking transition does not markedly depend on the excitation intensity, we can evaluate the D → B rate constant, $k^*_{D\to B}$, from the off-times:[41]

$$k^*_{D\to B}(d) = 1/\tau_{off}(d) \qquad (3)$$

On the other hand, the blinking on-time depends on the B → D transition rate, $k^*_{B\to D}$, as well as on the excitation rate, k^*_{exc}, for the photoactivation of the process:[44]

$$k_{on}(d) = k k^*_{excB\to D}(d)/[k_{rad}(d) + k_{nr}(d) + k^*_{B\to D}(d)] \qquad (4)$$

Because the intensity dependence of the on-times is well-

described by a fourth-power law under infrared excitation at 790 nm (see eq 2), the process leading to blinking seems to occur first through a transition to a high-energy excited state via a four-photon excitation and then through a transition from the excited bright state to a dark state. This suggestion is confirmed by the observation that, under 488 nm excitation, the blinking on-rate depends on the second power of the excitation intensity.

The evaluation of the blinking rate, $k^*_{B\rightarrow D}$ is then a matter of an estimate of the photoactivation rate k^*_{exc} whose order of magnitude can be evaluated only by assuming a four-photon cross-section $\sigma_{(4)} \cong \sigma_{(2)}{}^2\tau_{abs}$, where $\sigma_{(2)} \cong 1-100$ GM and $\tau_{abs} \cong 10^{-15}$ s are the typical cross-section and interaction times for the two-photon process.[32]

Now a plausible estimate of the fourth photon absorption cross-section is $\sigma_{(4)} \cong \sigma_{(2)}{}^2\tau_{abs} \cong 10^{-111}$ (cm^2 s)^4/s/photons^3,[32] similar to that ($\sigma_{(4)} \cong 10^{-109}$ (cm^2 s)^4/s/photons^3) measured for organic dyes.[45] The excitation rate, k^*_{exc}, can then be evaluated as:[46]

$$k^*_{exc} \cong 6.7 \times 10^{102} P^4_{\mu W} \sigma_{(4)} \qquad (5)$$

where $P_{\mu W}$ is the excitation power expressed in μW. At an average power of 400 μW ($<I_{exc}> \cong 100$ kW/cm^2), one estimates $k^*_{exc} \cong 300$ Hz for $\sigma_{(4)} \cong 10^{-111}$ (cm^2 s)^4/s/photons,[3] and this leads to values $k^*_{B\rightarrow D}$ on the order of a few hundreds of kHz. The uncertainty on the evaluation of $k^*_{B\rightarrow D}(d)$ can be made by assuming that the plausible range for $\sigma_{(4)}$ is $\cong 10^{-112}$—10^{-110} (cm^2 s)^4/s/photons^3. Both $k^*_{B\rightarrow D}(d)$ and $k^*_{D\rightarrow B}$ are shown in Figure 4D versus the gold NP diameter, at a laser intensity $\cong 100$ kW/cm^2. While $k^*_{D\rightarrow B}$ is on the order of a few Hz, $k^*_{B\rightarrow D}$ is found in the range of MHz to hundreds of kHz. Due to uncertainty in the prediction of the four-photon cross-section, our evaluation of the B $\rightarrow$ D transition is affected by a large variability (see Figure 4D). Nevertheless, the order of magnitude of $k^*_{B\rightarrow D}$ is likely to be much larger than that of $k^*_{D\rightarrow B}$. Moreover, we note that the $k^*_{B\rightarrow D}(d)$ and $k^*_{D\rightarrow B}(d)$ changes are approximately the same factor as a function of the NP size, although with opposite trends: $k^*_{D\rightarrow B}$ decreases with d, while $k^*_{B\rightarrow D}$ increases with d. Such an opposite trend points out that the forward and backward processes that lead to fluorescence blinking are inherently different. The forward process involves an interaction of a high-energy excited state of the fluorophore with the energetically accessible states within the (more or less)[47] continuous conduction band of the NP; the number of the conduction band states increases with the NP size.[47] On the other hand, the back process involves an interaction of a thermally relaxed electron on the bottom conduction state or on a local trap back with the HOMO of the molecule. It appears, therefore, reasonable that the back and forward processes that lead to fluorescence blinking depend differently on the NP size.[3]

What is the possible origin of the observed fluorescence blinking? The blinking time is too long, and repeated fluorescence imaging over the same area reveals no changes in the position of the observed molecule: triplet states and diffusional processes can, therefore, be ruled out.[41] The general absence, moreover, of large time fluctuations in the polarization of the fluorescence emission indicate that rotational dynamics is unlikely the source of the transient dark states.

One might be tempted to bring an electron-transfer process from the excited molecule to the gold surface as a possible explanation for the observed blinking: the dye stops fluorescence emission when it transfers an electron to gold and remains in the dark state (off) until the electron returns and the molecule comes back in the emission state (on). Indeed similar on- and off-times have been observed for perylene dyes on ITO surfaces,[18] while much faster relaxation rates have been indicated by excited-state lifetime measurements by Xie and Lu[17] for SM of cresyl violet lying on an ITO surface and for reductase when a tyrosine donates an electron to the excited flavin.[48]

To our knowledge, the present report is the first one in which fluorescence is monitored on such a wide time range to allow investigation of both slow (τ_{on} from blinking) and fast (k_{nr} from excited state decay) dynamics on the same dye system. Even the present results, however, do not provide clear evidence that may support univocally a photoactivated charge-transfer process. In fact, the observed blinking time scale, seconds, which can, however, be easily decreased to a few ms by increasing the excitation intensity, seem to be too long for dye−gold charge transfer. The slow off-times might be related also to the extremely large free mean path and lifetime of ballistic electrons in gold surfaces.[19] On the other hand, the relatively long on-times seem, at least in the present case, to be mostly determined by the slow excitation rate (eq 5) to the high-energy state from which dye−NP interactions occur, due to the fourth power dependence of k^*_{exc} on the excitation intensity at 790 nm.

An alternative origin to the fluorescence blinking could be a nonradiative energy transfer from the dye to the gold NPs that likely involves mixing between the dye high-energy excited-state electronic wave functions and the gold NP surface plasmons[5,49,50] or bound electronic transition dipoles.[38] The excited states might relax through a coupling with lattice vibrations and electronic levels of the metal surface,[51] such processes being modulated by the NP size[3].

Conclusions

We have provided a comprehensive picture of the photophysical behavior of an organic dye of the class of fluoresceins bound to gold NPs of various sizes, based on simultaneous SMS experiments at nanosecond (excited state lifetime) and millisecond (blinking) time resolution. The changes in the fluorescence emission dynamics of single SAMSA molecules bound to gold provide a clear indication for a strong coupling between the vibro-electronic configuration of the dye and the electronic and plasmonic features of the metal NP. We have observed frequent blinking events in the fluorescence traces collected from single dye molecules bound to gold NPs. Such a phenomenon is highly dependent on the excitation intensity (fourth power), indicating a nonlinear photoactivation. Though the process leading to blinking cannot univocally be identified, our data indicate that it could be due to an interaction between an excited (possible high energy) state of the dye with gold NP plasmon resonance and bound electronic transition dipoles. The evidence that the blinking relaxation rates, $k^*_{D\rightarrow B}$ and $k^*_{B\rightarrow D}$, are drastically lower (less than a few hundreds of kHz) with respect to k_{nr} (0.1 GHz), implies that the process leading to fluorescence blinking does not practically contribute to the measured shortening of the fluorescence lifetime.

The methodology and the findings reported here might also be of general relevance for the study of the interactions of organic compounds to metallic nanostructured surfaces that are essential in the construction of electro-optical molecular devices. Specifically, the electronic-plasmon coupling occurring at the excited states, probably at the origin of blinking, might be modulated by external biases, therefore, leading to possible molecular electronic applications.

Acknowledgment. The research reported in this work has been funded by the FIRB-MIUR Project "Molecular Nano-

devices" (to A.R.B., G.C., and S.C.), the PRIN-MIUR Project 2004−2005 (to A.R.B., S.C., and to G.C.), and a Fondazione Cariplo Project (to G.C.).

References and Notes

(1) Kamat, P. V. *J. Phys. Chem. B* **2002**, *106*, 7729.
(2) Eggeling, C.; Schaffer, J.; Seidel, C. A. M.; Korte, J.; Brehm, G.; Schneider, S.; Schrof, W. *J. Phys. Chem. A* **2001**, *105*, 3673.
(3) Link, S.; El-Sayed, A. *J. Phys. Chem. B* **1999**, *103*, 4212.
(4) Adams, D. M.; Brus, L.; Chidsey, C. E. D.; Creager, S.; Creutz, C.; Kagan, C. R.; Kamat, P. V.; Lieberman, M.; Lindsay, S.; Marcus, R. A.; Metzger, R. M.; Michel-Beyerle, M. E.; Miller, J. R.; Newton, M. D.; Rolison, D. R.; Sankey, O.; Schanze, K. S.; Yardley, J.; Zhu, X. Y. *J. Phys. Chem. B* **2003**, *107*, 6668.
(5) Stefani, F.; Gerbeth, G. *Phys. Rev. Lett.* **2005**, *94*, 023005.
(6) Dulkeith, E.; Morteani, A. C.; Niedereichholz, T.; Klar, T. A.; Feldmann, J.; Levi, S. A.; van Veggel, F. C. J. M.; Reinhoudt, D. N.; Möller, M.; Gittins, D. I. *Phys. Rev. Lett.* **2002**, *89*, 203002.
(7) Lakowicz, J. R.; Malicka, J.; D'Auria, S.; Gryczynski, I. *Anal. Biochem.* **2003**, *320*, 13.
(8) Anger, P. L.; Bharadwaj, P.; Novotny, L. *Phys. Rev. Lett.* **2006**, *96*, 113002.
(9) Kneipp, K.; Kneipp, H.; Itzkan, I.; Dasari, R. R.; Feld, M. S. *Chem. Rev.* **1999**, *99*, 2957.
(10) Michaels, A. M.; Nirmal, M.; Brus, L. E. *J. Am. Chem. Soc.* **1999**, *121*, 9932.
(11) Bizzarri, A. R.; Cannistraro, S. *Chem. Phys. Lett.* **2004**, *395*, 222.
(12) Cao, Y. C.; Jin, R. C.; Nam, J. M.; Thaxton, C. S.; Mirkin, C. A. *J. Am. Chem. Soc.* **2003**, *125*, 14676.
(13) Kelley, A. M.; Michalet, X.; Weiss, S. *Science* **2001**, *292*, 1671.
(14) Nie, S.; Emory, S. R. *Science* **1997**, *275*, 1102.
(15) Moerner, M.; Orritt, M. *Science* **1999**, *283*, 1670.
(16) Bizzarri, R.; Cannistraro, S. *Phys. Rev. Lett.* **2005**, *94*, 068303.
(17) Lu, H. P.; Xie, X. S. *J. Phys. Chem. B* **1997**, *101*, 2753−2757.
(18) Holman, M. W.; Adams, D. M. *ChemPhysChem* **2005**, *5*, 1831−1836.
(19) Grätzel, M. *Nature* **2003**, *421*, 586.
(20) Willner, I.; Katz, E. *Angew. Chem., Int. Ed.* **2000**, *39*, 1180.
(21) Freeman, R. G.; Grabar, K. C.; Allison, K. J.; Bright, R. M.; Davis, J. A.; Guthrie, A. P.; Hommer, M. B.; Jackson, M. A.; Smith, P. C.; Walter, D. G.; Natan, M. *J. Science* **1995**, *267*, 1629.
(22) Kirk, J. S.; Bohn, P. W. *J. Am. Chem. Soc.* **2004**, *126*, 5920.
(23) Hildebrandt, P.; Stockburger,M. *J. Raman Spectrosc.* **1986**, *17*, 55.
(24) Diaspro, A.; Chirico, G. In *Advances in Imaging and Electron Physics*; Hawkes, P., Ed.; Elsevier Science: New York, 2003; Vol. 126, p 193.
(25) Malengo, G.; Milani, R.; Cannone, F.; Krol, S.; Diaspro, A.; Chirico, G. *Rev. Sci. Instrum.* **2004**, *75*, 2746.
(26) Ulman, A. *Chem. Rev.* **1996**, *96*, 1533.
(27) Lettinga, M. P.; Han, Z. H.; van Zandvoort, M. A. M. J. *Phys. Chem. Chem. Phys.* **2000**, *2*, 3697.
(28) Fleury, L.; Segura, J. M.; Zumofen, G.; Hecht, B.; Wild, U. P. *Phys. Rev. Lett.* **2000**, *84*, 1148.
(29) Hollars, C. W.; Lane, S. M.; Huser, T. *Chem. Phys. Lett.* **2003**, *370*, 393.
(30) Sjoerback, R.; Nygren, J.; Kubista, M. *Spectrochim. Acta A*-Molecular and Biomolecular Spectroscopy **1995**, *51*, L7.
(31) Deconvolution of the fluorescence decay with the intensity response function, whose fwhm value is ≅ 700 ps, was performed to obtain the excited-state lifetime.
(32) Xu, C. Cross-sections of Fluorescence Molecules in Multiphoton Microscopy. In *Confocal and Two-photon Microscopy, Foundations, applications and Advances*; Diaspro, A., Ed.; Wiley-Liss: New York, 2002; Chapter 4, p 75.
(33) Cannone, F.; Chirico, G.; Baldini, G.; Diaspro, A. *J. Microsc.* **2003**, *210*, 149.
(34) Xu, C.; Webb, W. W. *J. Opt. Soc. Am. B* **1996**, *13*, 481.
(35) Gryczynski, I.; Malicka, J.; Shen, Y.; Gryczynski, Z.; Lakowicz, J. R. *J. Phys. Chem. B* **2002**, *106*, 2191.
(36) Ipe, B. I.; Thomas, K. G.; Barazzouk, S.; Hotchandani, S.; Kamat, P. V. *J. Phys. Chem. B* **2002**, *106*, 18.
(37) Gersten, J.; Nitzan, A. *J. Chem. Phys.* **1981**, *75*, 1139.
(38) Wiederrecht, G.; Wurtz, G. A.; Hranisavljevic, J. *Nano Lett.* **2004**, *4*, 2121.
(39) Baldini, G.; Cannone, F.; Chirico, G. *Science* **2005**, *309*, 1096.
(40) Chirico, G.; Cannone, F.; Baldini, G.; Diaspro, A. *Biophys. J.* **2003**, *84*, 588.
(41) Holman, M. W.; Liu, R.; Adams, D. M. *J. Am. Chem. Soc.* **2003**, *125*, 12649.
(42) Briefly, the histogram of the photon counts per sampling time displays two maxima, one at ≅0 counts in our case, well-separated by a minimum that is taken as a threshold value to discriminate between the on and off states.
(43) Lakowicz, J. R. *Anal. Biochem.* **2005**, *337*, 171.
(44) Yip, W. T. *J. Phys. Chem. A* **1998**, *102*, 7564.
(45) Hernandez, F. E.; Belfield, K. D.; Cohanoschi, I.; Balu, M.; Schafer, K. J. *Appl. Opt.* **2004**, *43*, 5394.
(46) By taking the excitation wavelength $\lambda = 790$ nm, laser pulse width $\tau = 230 \pm 30$ fs, objective numerical aperture NA = 1.3, and laser repetition rate $f = 80$ MHz, one can compute the excitation rate for a four-photon excitation process as $k_{exc} = \sigma_4[(\langle P\rangle_{\mu W}{}^4/(f\tau\pi hc\lambda)^4)(NA^8/(0.61)^8)] \times 10^{-16}$, where h and c are the Planck constant and the light speed, and the average laser power $\langle P\rangle_{\mu W}$ and $\sigma_{(4)}$ are expressed in μW and photons^{-3} cm^8 s^3, respectively.
(47) Parak, W. J.; Manna, L.; Simmel, F. C.; Gerion, S.; Alivisatos, P. In *Nanoparticles: form theory to applications*; Schimd, G., Ed.; Wiley-VCH: Weinheim, Germany, 2004; p 4.
(48) Yang, H. G.; Luo, G. B.; Karnchanaphanurach, P.; Louie, T. M.; Rech, I.; Cova, S.; Xun, L. Y.; Xie, X. S. *Science* **2003**, *302*, 262.
(49) Liebermann, T.; Knoll, W. *Colloids Surf., A* **2000**, *171*, 115.
(50) Vasilev, K.; Knoll, W.; Kreiter, M. *J. Chem. Phys.* **2004**, *102*, 3439.
(51) Makarova, O. V.; Ostafin, A. E.; Miyoshi, H.; Norris, J. R., Jr.; Meisel, D. *J. Phys. Chem. B* **1999**, *103*, 9080.